Dual roles of ATM in the cellular response to radiation and in cell growth control

Yang Xu and David Baltimore[1]

Department of Biology, Massachusetts Institute of Technology, Cambridge, Massachusetts 02139 USA

The gene mutated in ataxia-telangiectasia (AT) patients, denoted *ATM*, encodes a putative protein or lipid kinase. To elucidate the functions of ATM, we disrupted the mouse *ATM* gene through homologous recombination in mice. Consistent with cellular defects of AT patients, the $ATM^{-/-}$ cells are hypersensitive to γ-irradiation and defective in cell-cycle arrest following radiation, correlating with a defective up-regulation of p53. In addition, $ATM^{-/-}$ mouse thymocytes are more resistant to apoptosis induced by γ-irradiation than normal thymocytes. $ATM^{-/-}$ fibroblasts are inefficient in G_1 to S-phase progression following serum stimulation and senesce after only a few passages in culture. They have an increased constitutive level of $p21^{CIP1/WAF1}$. The ATM protein is therefore critical both for cellular responses to ionizing radiation and for normal cell-cycle progression. $ATM^{+/-}$ fibroblasts and thymocytes showed intermediately defective responses to irradiation but no growth defect, suggesting that the increased cancer risk of AT heterozygotes could be attributable to poor checkpoint function.

Ataxia-telangiectasia (AT) is an autosomal recessive human hereditary disorder characterized by multisystem defects. These include progressive cerebellar degeneration leading to ataxia, dilated blood vessels (telangiectasia) in the eye and facial area, sensitivity to γ-irradiation, high incidence of tumorgenesis in the lymphoid system, degeneration of thymus, and deficiency in both humoral and cellular immune responses (Lehmann 1982; Swift et al. 1991; Thacker 1994). Whereas AT patients are relatively rare (about 4×10^{-4}), about 0.5% of the general population harbors a single mutant allele (Swift et al. 1987, 1991). Significantly, cells derived from people heterozygous for an AT mutation have an intermediate sensitivity to γ-irradiation, and it has been suggested that heterozygous people have a cancer predisposition about fivefold that of the normal population (Swift et al. 1987, 1991). Therefore, understanding the molecular basis of the AT mutation is of great importance.

AT cells are hypersensitive to DNA damaging reagents, such as γ-irradiation and restriction enzyme digestion, that can introduce double-stranded DNA breaks (Thacker 1994). Furthermore, the ability of AT cells to arrest in G_1 following DNA damage is deficient, indicating defects in the cell-cycle checkpoint control (Meyn 1995). Because the induction of the p53 protein after γ-irradiation is responsible for the arrest at G_1 checkpoint

(Kuerbitz et al. 1992), studies have been carried out to evaluate the p53 response to γ-irradiation in human AT cells. The initial study suggested that the p53 response to γ-irradiation is defective in AT cells (Kastan et al. 1992). However, later studies found either no substantial defect in the p53 response to γ-irradiation in AT cells or that the p53 response is reduced with a delayed kinetics (Khanna and Lavin 1993; Lu and Lane 1993). Genetic heterogeneity among mutant and control cells may have masked effects.

A gene mutated in all tested AT patients, denoted *ATM*, has been identified recently through positional cloning (Savitsky et al. 1995). The *ATM* gene encodes a large protein that is similar to a number of large proteins that define a subfamily of kinases including the PI-3 (lipid) kinase (Savitsky et al. 1995). Members of this family contain a highly conserved carboxy-terminal kinase domain (Zakian 1995). Several members of this family, including yeast proteins Rad3, Mec1, and Tel1, are involved in DNA repair and cell-cycle checkpoint control (Weinert and Lydall 1993; Greenwell et al. 1995; Hari et al. 1995; Morrow et al. 1995; Paulovich and Hartwell 1995). Other members of the family, such as yeast proteins Tor1p and Tor2p and their mammalian counterpart FRAP, control cell-cycle progression from the G1 phase into the S phase (Brown et al. 1995). A direct link between this kinase family and DNA repair was provided by the discovery that the DNA-dependent protein kinase (DNA-PK) is a member of this family (Hartley et al.

[1]Corresponding author.

1995). It is involved in double-stranded DNA break repair and in lymphocyte V(D)J recombination—a defective DNA-PK leads to severe immunodeficiency in mice (Blunt et al. 1995). If structural homology implies functional similarity, ATM could be involved in a cell-cycle checkpoint responding to DNA damage.

The PI-3 kinase family members, including p110α, β, and γ, phosphorylate inositol phospholipids that are involved in signal transduction pathways (Hunter 1995). Members of the ATM kinase family have so far failed to show any intrinsic lipid kinase activity (Hunter 1995). However, Tor proteins and DNA-PK, as well as PI-3 kinase, display protein kinase activity (Carpenter et al. 1993; Dhand et al. 1994; Brown et al. 1995; Hartley et al. 1995), suggesting that ATM may function as a protein kinase.

To elucidate the mechanisms of defective cell-cycle checkpoint control, neurodegeneration, and immunodeficiency in AT patients, we created mutant mice in which the *ATM* gene is disrupted through homologous recombination. The $ATM^{-/-}$ mice are viable and have developed immune and other defects similar to certain symptoms of AT patients (Xu et al., this issue). Our study of mouse embryo fibroblasts (MEFs) and thymocytes from mice indicates a dual role of ATM relating to cell-cycle checkpoint control. Following γ-irradiation, the $ATM^{-/-}$ cells arrest cell cycle poorly and have a defective p53 response. These characteristics support the idea that ATM is responsible for signaling the p53-mediated cell-cycle arrest that follows ionizing radiation. Similarly, ATM was found to be required for efficient apoptosis of thymocytes following γ-irradiation, another p53-mediated response. ATM is also required for efficient G_1- to S-phase transition during cell-cycle progression. Furthermore, $ATM^{-/-}$ cells prematurely senesce and their level of $p21^{CIP1/WAF1}$ protein is chronically high. Thus, ATM also plays a critical role in cellular proliferation.

Results

Targeted disruption of the ATM gene in mice

Because the kinase domain of ATM is frequently mutated in AT patients—alteration of one serine residue in the domain can cause the AT phenotype (Savitsky et al. 1995)—we designed a targeting construct to disrupt conserved sequence in the ATM kinase domain (Fig. 1A,B). To screen for homologous recombination events, genomic DNA isolated from transfected embryonic stem (ES) clones was digested with *Bam*HI and probed with probe A that was outside the transfected targeting construct, giving a 18-kb germ-line band and a 10-kb mutant band (Fig. 1A–C). Positive ES clones were further confirmed by *Bam*HI digestion and hybridization to probe B, giving a 18-kb germ-line band and a 4.3-kb mutant band (Fig. 1A–C).

To generate $ATM^{-/-}$ ES cells, the $ATM^{+/-}$ ES cells were selected with higher concentrations of G418 as described previously (Xu et al. 1996b). ES colonies surviv-
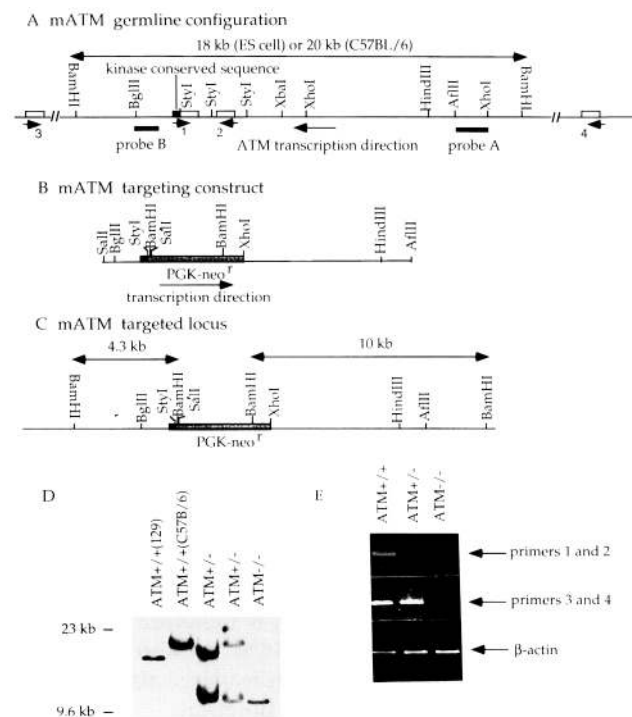
Figure 1. Targeted disruption of the *ATM* gene in mice. (*A*) Genomic configuration of the germ-line *ATM* locus. Exons are represented with open boxes except that the exonal region encoding the conserved kinase sequence is represented with a filled box. The length of the *Bam*HI diagnostic restriction fragment and the locations of the probes are shown. The transcriptional direction of the *ATM* gene and the locations of the primers are indicated with arrowheads. (*B*) Targeting construct to insert the PGK-neo^r gene into one *ATM* exon and simultaneously to replace the second exon. The transcriptional direction of the PGK-neo^r gene is indicated with an arrowhead and is opposite that of the *ATM* gene. (*C*) Targeted locus following homologous recombination between the targeting construct and the endogenous *ATM* locus. The lengths of the diagnostic restriction fragments are shown. (*D*) Southern blot analysis of the tail DNA from $ATM^{+/+}$, $ATM^{+/-}$, and $ATM^{-/-}$ mice. Tail DNA (10 μg) was digested with *Bam*HI and hybridized to probe A. Because of the polymorphoric nature of the *Bam*HI restriction at this locus, the size of the germline band is either 18 kb if the allele is derived from ES cells or 20 kb if the allele is derived from C57BL/6. The locations of the DNA size marker are indicated. (*E*) RT–PCR analysis of the *ATM* mRNA in $ATM^{+/+}$, $ATM^{+/-}$, and $ATM^{-/-}$ MEFs. The amplified products from the synthesized cDNA are correlated with the primers indicated with arrowheads.

ing the selection of 4.8 mg/ml G418 were expanded and analyzed by Southern blotting. The $ATM^{-/-}$ ES cells were subcloned and confirmed (data not shown).

Six out of seven $ATM^{+/-}$ ES clones injected into blastocysts gave rise to chimeric mice that transmitted the *ATM* mutation into germ-line. Mice heterozygous for the *ATM* mutation ($ATM^{+/-}$) were intercrossed to generate mice homozygous for the *ATM* mutation ($ATM^{-/-}$). Tail DNA derived from $ATM^{+/+}$, $ATM^{+/-}$,

and $ATM^{-/-}$ mice were analyzed by Southern blot (Fig. 1D).

Because the *ATM* gene is expressed ubiquitously (Savitsky et al. 1995), we employed RT–PCR to check the expression of *ATM* in the MEFs derived from day-14 $ATM^{+/+}$, $ATM^{+/-}$, and $ATM^{-/-}$ embryos. In the PCR assays, primers 1 and 2 were used to detect the coding region that was disrupted directly by the PGK-neo^r gene; primers 3 and 4 were outside the targeting construct and used to amplify a larger coding region containing the disrupted exons (Fig. 1A). Using both sets of primers, no expression of the *ATM* mRNA could be detected in the $ATM^{-/-}$ MEFs (Fig. 1E), indicating that the expression of the ATM kinase domain had been disrupted. Because the ATM kinase domain appears to be essential for the function of ATM, this targeted mutation should destroy the production of a functional ATM.

$ATM^{-/-}$ ES cells are hypersensitive to γ-irradiation

Taking advantage of the capability of ES cells to grow clonally, we established a clonogenic survival assay to examine the sensitivity of $ATM^{-/-}$ ES cells to γ-irradiation. Consistent with cellular hypersensitivity of AT cells, the $ATM^{-/-}$ ES cells are also much more sensitive to the γ-irradiation than $ATM^{+/+}$ and $ATM^{+/-}$ ES cells (Fig. 2).
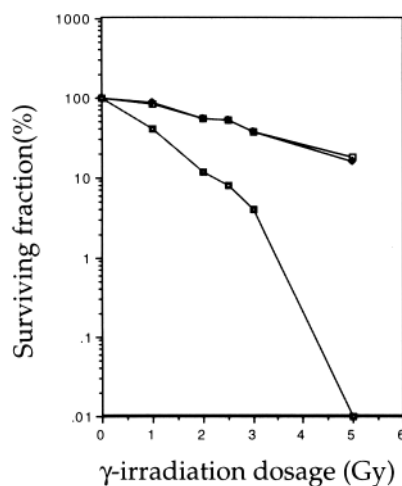
Cell-cycle arrest following irradiation

In response to DNA damage caused by agents such as γ- or UV irradiation, mammalian cells undergo cell-cycle G_1 arrest (Kastan et al. 1992; Lu and Lane 1993). However, inhibition of cell-cycle progression by γ-irradiation is reduced in cells derived from AT patients

Figure 2. Clonogenic survival of $ATM^{+/+}$ (□), $ATM^{+/-}$ (♦), and $ATM^{-/-}$ (■) ES cells following exposure to graded doses of γ-irradiation. For each irradiation dosage, colonies from duplicated wells were counted. The genotypes are indicated in the figure. Consistent results were obtained from two sets of independently produced $ATM^{+/-}$ and $ATM^{-/-}$ ES cells.

(Meyn 1995). Therefore, we examined the ability of $ATM^{+/+}$, $ATM^{+/-}$, and $ATM^{-/-}$ MEFs to arrest cell cycle at G_1 following γ-irradiation or UV irradiation using a protocol originally developed by others (Kastan et al. 1991, 1992; Kuerbitz et al 1992). The cells were asynchronously growing at the time of irradiation and their cell-cycle position was assayed using the fluorescence-activated cell analyzer to measure DNA content and bromodeoxyuridine (BrdU) incorporation during a pulse label at 14 hr after irradiation. In the absence of irradiation, the $ATM^{-/-}$ and $ATM^{+/-}$ cells had somewhat smaller S-phase fractions than the wild-type cells (Fig. 3A; not shown). In normal cells, there was a 75% loss of S-phase cells following irradiation of 10 Gy and an accumulation of cells in G_2/M and G_1/G_0 (Fig. 3A). The $ATM^{-/-}$ MEFs had only about a 40% loss of S-phase at this dose of irradiation. G_2/M phase cells accumulated extensively but there were relatively fewer G_1/G_0 cells (Fig. 3A,B). The effects on S-phase cells were dose-dependent (Fig. 3B). The $ATM^{+/-}$ MEFs exhibited an intermediate defect in cell-cycle arrest following higher dosages (≥ 5 Gy; Fig. 3A,B), but apparently behaved normally if exposed only to a lower dose (2 Gy; data not shown). In contrast, $ATM^{+/+}$, $ATM^{+/-}$, and $ATM^{-/-}$ MEFs showed equivalent ability to reduce their S-phase fraction following UV-irradiation (Fig. 3B).
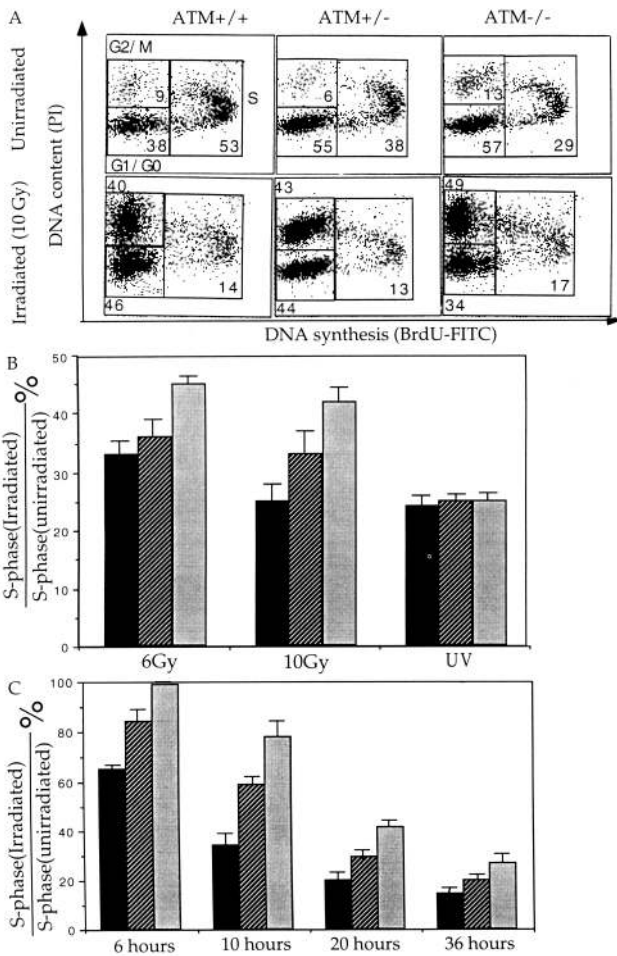
To measure the optimal defect of $ATM^{-/-}$ MEFs in G_1 cell-cycle arrest following γ-irradiation, we examined the ability of $ATM^{+/+}$, $ATM^{+/-}$, and $ATM^{-/-}$ MEFs to arrest their cell cycle in G_1 phase at different time points following 10-Gy γ-irradiation. Whereas maximal defects in G_1 arrest were observed 10 hr following γ-irradiation, $ATM^{-/-}$ MEFs exhibited defective G_1 cell-cycle arrest and $ATM^{+/-}$ MEFs showed an intermediate defect at all tested time points following γ-irradiation (Fig. 3C).

The p53 response to DNA damage

The p53 protein level is up-regulated transiently after DNA damage and cell-cycle arrest following DNA damage requires an intact p53 gene (Kastan et al. 1992). The role of p53 may be to activate the expression of a number of genes including $p21^{CIP1/WAF1}$ (El-Diery et al. 1993; Xiong et al. 1993; Macleod et al. 1995). To understand the basis of the defective cell-cycle G_1 arrest following γ-irradiation but not UV-irradiation in $ATM^{-/-}$ cells, the protein levels of p53 at different time points following γ- or UV irradiation were evaluated by immunoblot analysis of whole-cell extracts. It was confirmed that equivalent amounts of protein were transferred in each lane by staining the nitrocellulose membrane after transfer. One hour following 10 Gy γ-irradiation, a significant increase of p53 protein was seen in both $ATM^{+/+}$ and $ATM^{+/-}$ MEFs (Fig. 4A), although the magnitude of the up-regulation in $ATM^{+/-}$ MEFs appeared to be less than that in $ATM^{+/+}$ MEFs. The p53 protein levels decreased at later time points (2, 3, 4, 5, 8 hr) following γ-irradiation in both $ATM^{+/+}$ and $ATM^{+/-}$ MEFs (Fig. 4A, data not shown). In contrast, no increase of p53 protein level

ation (Fig. 4A; data not shown). Therefore, the p53 response to γ-irradiation was defective in $ATM^{-/-}$ cells.

Based on the reported kinetics of the p53 response to UV-irradiation in mouse cells (Lu and Lane 1993), we analyzed the p53 response in MEFs 14 hr following UV irradiation (Fig. 4B; data not shown). A similar up-regulation of p53 protein level was observed in MEFs of all genotypes (Fig. 4B), indicating that the p53 response to UV irradiation is normal in $ATM^{-/-}$ MEFs.

p21 expression in MEFs

We also analyzed the p21 protein levels in $ATM^{+/+}$, $ATM^{+/-}$, and $ATM^{-/-}$ MEFs. The specificity of the polyclonal anti-p21 antibody we used has been verified previously (Deng et al. 1995). A considerably higher level of p21 protein was detected in both proliferating and resting $ATM^{-/-}$ MEFs (Fig. 4C). In addition, analysis of the p21 protein level at different time points following serum stimulation of synchronously growth-arrested cells also indicated higher levels of p21 protein at all time points in $ATM^{-/-}$ MEFs (Fig. 4D). p21 protein lev-

Figure 3. Defective ability of the $ATM^{-/-}$ MEFs to arrest in G_1 phase following γ-irradiation. (A) A FACScan analysis of the untreated and irradiated $ATM^{+/+}$, $ATM^{+/-}$, and $ATM^{-/-}$ MEFs following 10 Gy γ-irradiation. DNA synthesis is revealed by FITC-conjugated anti-BrdU antibody and the DNA content is revealed by propidium iodide (PI) staining. Boxes representing cells in G_1, S, and G_2/M phases as well as the percentage of total cells are indicated. We have not observed consistent difference between the number of S-phase cells of $ATM^{+/+}$ and $ATM^{+/-}$ MEFs. (B) Quantitative analysis of the number of cells in S phase following γ-irradiation versus the number of cells in S phase in an untreated control. (Solid bar) $ATM^{+/+}$; (hatched bar) $ATM^{+/-}$; (gray bar) $ATM^{-/-}$. Three independent experiments were performed for γ-irradiation at each dosage and two for UV-irradiation at a dosage of 60 J/M². The mean value is presented with error bars showing standard derivation. Consistent results were obtained from independently derived MEFs. (C) Quantitative analysis of the number of cells in S phase following γ-irradiation versus the number of cells in S phase in an untreated control 6, 10, 20, 36 hr following 10 Gy γ-irradiation. Bars as in B. Three independent experiments were performed and mean value is presented with error bars showing standard deviation.

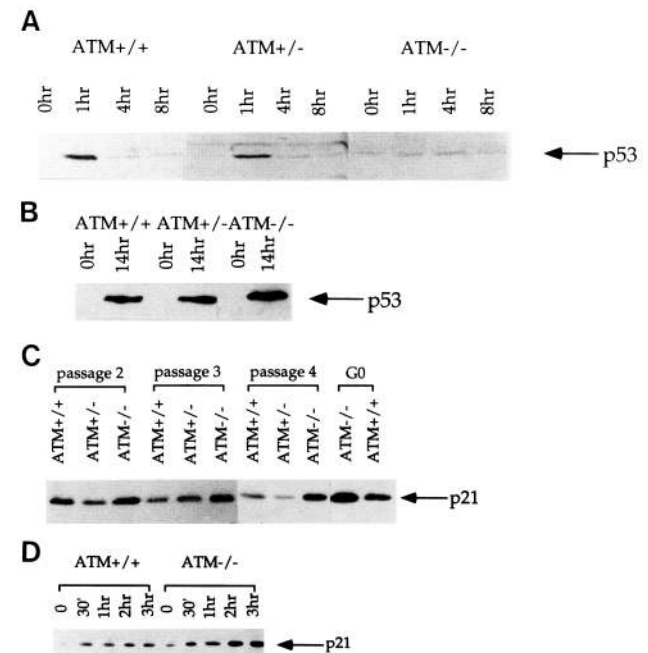**Figure 4.** The p53 response to radiation and p21 protein levels in $ATM^{+/+}$, $ATM^{+/-}$, and $ATM^{-/-}$ MEFs. (A) The protein levels of p53 at 0, 1, 4, 8 hr following 10-Gy γ-irradiation. The lanes are labeled on the top. p53 is indicated with arrowheads. (B) The protein levels of p53 at 0 and 14 hr following 60 J/m² UV-irradiation. The lanes are labeled at the top and protein indicated with arrowheads. (C) The p21 protein level in proliferating and resting MEFs. Proliferating MEFs of various passage number were harvested and MEFs resting at G_0 were obtained by serum starvation for 96 hr. The genotypes and passage numbers are shown on the top and p21 is indicated with an arrowhead. (D) Protein levels of p21 at different time points after serum stimulation of G_0 MEFs. The time points and genotypes are shown on the top and p21 is indicated with arrowheads.

was observed in $ATM^{-/-}$ MEFs 1 hr after γ-irradiation and only a small increase of p53 protein level was detected at 3 or 4 hr but not at 2, 5, 8 hr following irradi-

els in cells derived from AT patients have been examined (Canman et al. 1994). However, no difference was detected between AT cells and cells derived from normal individuals. This could be attributable to a difference between human and mouse cells or the fact that the AT cells used in these studies were immortalized and EBV-immortalization may mask this p21 effect.
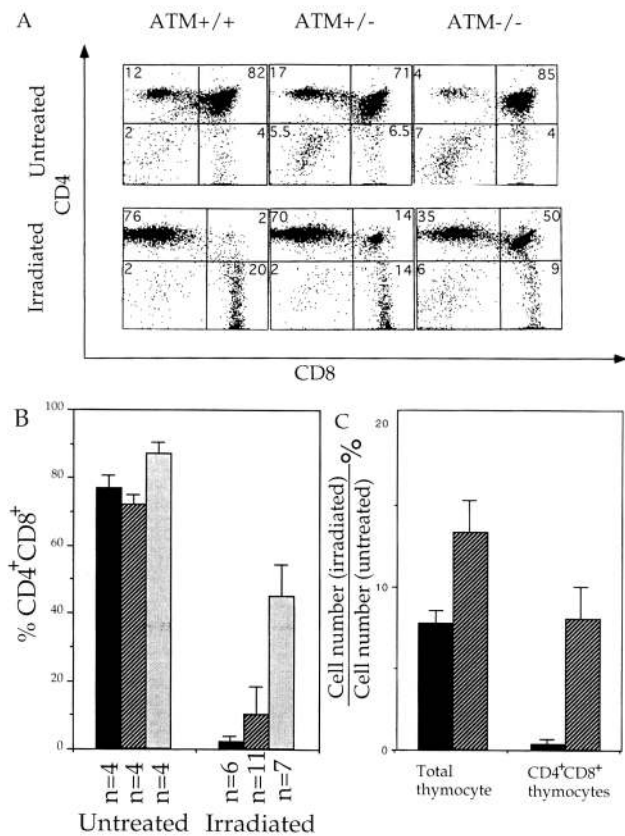
γ-irradiation-induced apoptosis of thymocytes in vivo

Because γ-irradiation-induced apoptosis of immature thymocytes is mediated by p53 (Clarke et al. 1993; Lowe et al. 1993) and the p53 response to γ-irradiation is defective in $ATM^{-/-}$ MEFs (Fig. 4A), we examined the apoptotic response of $ATM^{+/-}$ and $ATM^{-/-}$ thymocytes to in vivo γ-irradiation. T-cell development in the thymus of both $ATM^{+/-}$ and $ATM^{-/-}$ mice is defective and will be described in detail elsewhere (Fig. 5A; Xu et al., this issue). As expected, the immature $CD4^+CD8^+$ thymocytes, which are most susceptible to apoptosis, essentially disappear in the thymus of normal mice 48 hr after exposure to 5-Gy γ-irradiation (Smith et al. 1989; Clarke et al. 1993; Lowe et al. 1993; Fig. 5A–C). Similar to $ATM^{+/+}$ mice, total thymocyte number is also reduced significantly in $ATM^{-/-}$ mice 48 hr after exposure to γ-irradiation, indicating that $ATM^{-/-}$ thymocytes are also sensitive to γ-irradiation (Fig. 5C). However, compared with that of $ATM^{+/+}$ mice, the much higher percentage of immature thymocytes surviving the effect of γ-irradiation in $ATM^{-/-}$ mice indicates that $ATM^{-/-}$ immature thymocytes are more resistant to the effects of γ-irradiation than normal immature thymocytes, implying that p53-mediated apoptosis following γ-irradiation is defective in $ATM^{-/-}$ thymocytes (Fig. 5A–C). $ATM^{+/-}$ thymocytes displayed an intermediate resistance to γ-irradiation (Fig. 5A,B).

Impaired proliferation of $ATM^{-/-}$ MEFs in cultures

Fibroblasts derived from AT patients display a premature senescence (Shiloh et al. 1985). Therefore, we examined the growth properties of $ATM^{+/+}$, $ATM^{+/-}$, and $ATM^{-/-}$ MEFs. Irrespective of their passage numbers, $ATM^{-/-}$ MEFs proliferated more slowly than $ATM^{+/+}$ and $ATM^{+/-}$ MEFs (Fig. 6A,B). In addition, and in contrast to p53$^{-/-}$ MEFs, the saturation density of $ATM^{-/-}$ MEFs is only about half that of $ATM^{+/-}$ and $ATM^{+/+}$ MEFs (Fig. 6A,B; Deng et al. 1995). After passage 6, the $ATM^{-/-}$ MEFs essentially became senescent, whereas the $ATM^{+/-}$ and $ATM^{+/+}$ MEFs continued to proliferate (Fig. 6C).

G_1/S progression in the cell cycle of $ATM^{-/-}$ MEFs

To examine the defects in cellular growth involved in the slow proliferation and ultimate senescence of the mutant fibroblasts, we asked how efficiently the cells came into S phase after serum stimulation. $ATM^{+/+}$, $ATM^{+/-}$, and $ATM^{-/-}$ MEFs of passage 3 synchronized at G_0 by serum starvation were released into medium


Figure 5. γ-irradiation-induced apoptosis of mouse thymocytes. (A) Thymocytes were derived from $ATM^{+/+}$, $ATM^{+/-}$, and $ATM^{-/-}$ mice either exposed to γ-irradiation (5 Gy; bottom) or without any treatment (top) and analyzed for the expression of CD4 or CD8 surface markers. The percentage of subpopulations of thymocytes is indicated. (B) Mean percentage of immature $CD4^+CD8^+$ thymocytes in $ATM^{+/+}$ (solid bar), $ATM^{+/-}$ (hatched bar), and $ATM^{-/-}$ (gray bar) mice 48 hr after exposure to 5-Gy γ-irradiation or no treatment. n represents the number of mice analyzed. (C) Thymocyte reduction following γ-irradiation. Thymocytes were recovered from $ATM^{+/+}$ (solid bar) and $ATM^{-/-}$ (hatched bar) mice 48 hr after exposure to 5-Gy γ-irradiation. Thymocytes were also recovered from littermates or same-aged mice without irradiation treatment. Five sets of irradiated and untreated mice of each genotype were analyzed and percentile ratio of thymocyte number derived from irradiated versus untreated mice is presented with error bars showing standard deviation.

containing 10% fetal calf serum and 24 or 72 hr later the percentage of cells in S phase was determined. Compared with $ATM^{+/+}$ and $ATM^{+/-}$ MEFs, a considerably lower percentage of $ATM^{-/-}$ cells had entered the S phase 24 hr after serum stimulation (Fig. 7A,B). However, >90% of $ATM^{+/+}$ and $ATM^{-/-}$ MEFs had entered the S phase by 72 hr (data not shown). Therefore, $ATM^{-/-}$ MEFs have a defective ability to enter S phase, probably accounting for their slower growth.

Discussion

Previous work had demonstrated a number of defects in
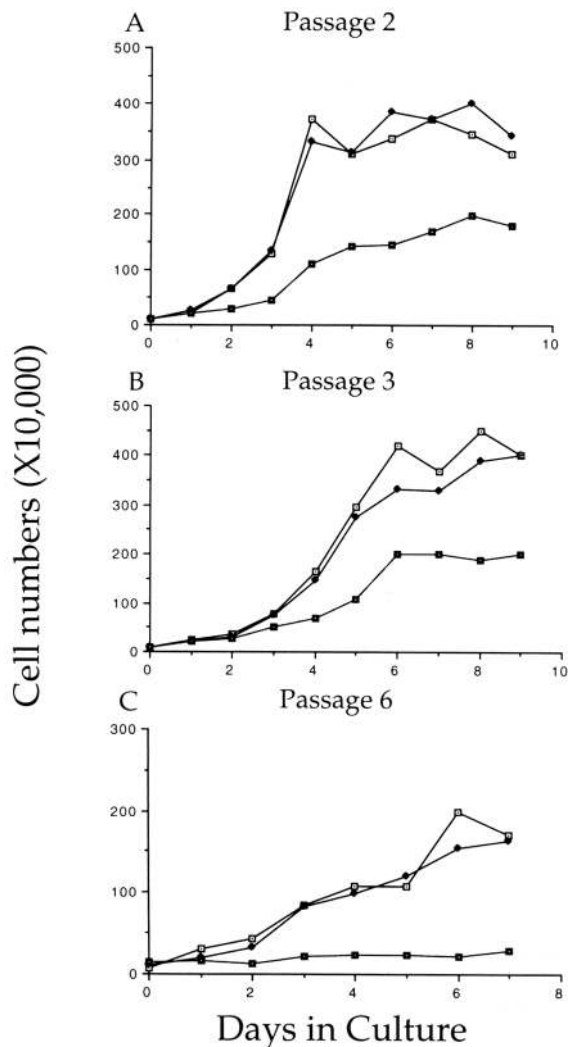
Figure 6. Proliferation curves and saturation density of $ATM^{+/+}$ (□), $ATM^{+/-}$ (◆), and $ATM^{-/-}$ (■) MEFs at (A) passage 2, (B) passage 3, and (C) passage 6. The cell number represents the average of the three plates counted at each time point. The genotypes and passage numbers are indicated in the figure.

$ATM^{-/-}$ human cells derived from patients, but there was disagreement in the literature about their nature, probably as a consequence of the genetic heterogeneity inherent in human studies. In particular, it is not clear that all human ATM alleles give the same phenotype. Using $ATM^{-/-}$ cells derived from mice with a disrupted ATM gene, we could confirm certain previous studies and provide a clear picture of two types of defects in the cells, one for the response to ionizing radiation and the other in normal growth control. As significantly, we could demonstrate a series of defects in $ATM^{+/-}$ cells that might explain an increased tendency to carcinogenesis in heterozygous individuals.

Studying the response of cells to γ-irradiation, we found that—consistent with previous studies of fibroblasts derived from AT patients (Meyn 1995)—the

$ATM^{-/-}$ cells do not arrest as effectively as wild-type cells. They maintain more S-phase cells after irradiation, indicating a lack of an effective block at the G_1/S border. They were not defective in their response to UV irradiation. Thus, ATM behaves as a checkpoint controller for cells that have been exposed to ionizing radiation, perhaps indicating that the protein is involved in sensing the DNA strand breaks caused by the irradiation. An important conclusion from these studies is that in the absence of ATM function, γ-irradiation does not induce p53 effectively. This indicates that p53 is downstream of ATM.

Consistent with studies of human AT cells, ES cells that are $ATM^{-/-}$ are more sensitive to γ-irradiation than normal ES cells. A defective ability of AT cells to cell-cycle arrest following DNA damage has been suggested previously to contribute to the hypersensitivity of AT cells to ionizing radiation and the high frequency of tumorgenesis in AT patients (Lehmann 1982; Shiloh et al. 1985).

Paradoxically, $ATM^{-/-}$ CD4$^+$CD8$^+$ thymocytes that have been irradiated in situ are more resistant to γ-irradiation than their wild-type counterparts but this probably indicates that ATM is involved in signaling an apoptotic response in some cells and a growth arrest re-
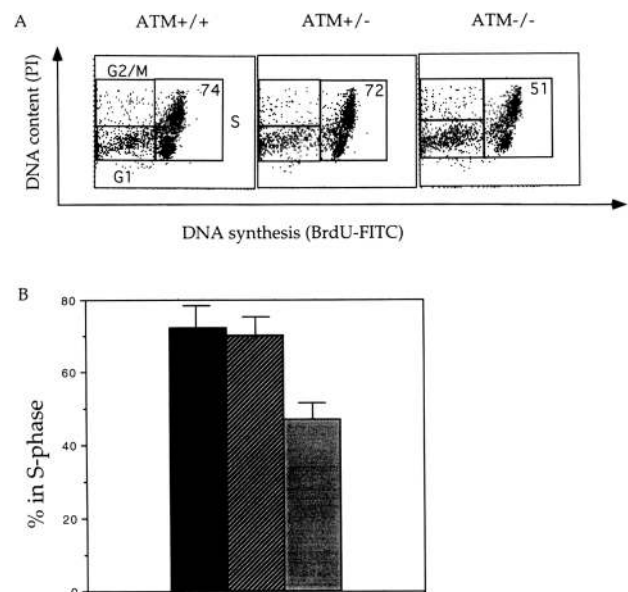
Figure 7. S-phase entry following serum stimulation of synchronized $ATM^{+/+}$, $ATM^{+/-}$, and $ATM^{-/-}$ MEFs. (A) FACScan analysis of synchronized MEFs after serum stimulation. Serum-starved $ATM^{+/+}$, $ATM^{+/-}$, and $ATM^{-/-}$ MEFs were released into DMEM containing 10% FBS for 24 hr and harvested. The S-phase cells (BrdU$^+$) are revealed with FITC-conjugated anti-BrdU and DNA content is revealed with propidium iodide. Boxes representing cells in G_0/G_1, S, and G_2/M phases and percentages of cells in S phase are indicated. (B) Quantitative analysis of the percentage of S-phase cells after serum stimulation of synchronized $ATM^{+/+}$ (solid bar), $ATM^{+/-}$ (hatched bar), and $ATM^{-/-}$ (gray bar) MEFs. Three independent experiments were carried out and the mean value with error bars are presented.

sponse in others, just as seen for p53 signaling (Clarke et al. 1993; Lowe et al. 1993).

ATM appears to play a key role in normal control of fibroblast growth. MEFs from $ATM^{-/-}$ mice showed three defects in in vitro growth: a lower saturation density, slow passage through the G_1/S border after serum stimulation, and a more rapid senescence. Fibroblasts derived from AT patients (Shiloh et al. 1985) display an apparent premature senescence. In addition, $ATM^{-/-}$ mouse cells also showed a higher than normal constitutive level of p21 at all times. What causes the increased p21 is not clear, and whether it is the cause of the various effects on cell growth must be tested, but the correlation of increased p21 and senescence has been noted before (Halevy et al. 1995; Nakanishi et al. 1995; Parker et al. 1995).

$ATM^{+/-}$ cells showed partial defects in certain parameters we measured but not others. In particular, they were unaltered in their sensitivity to γ-irradiation, but that was only measured in ES cells at a low radiation dose ($\leq$5 Gy); they showed a partial defect in cell-cycle arrest at high doses of ionizing radiation; their radiation-induced p53 response was lower than wild-type; they showed some resistance to thymocyte death; but their in vitro growth parameters were unaffected. The defects are probably not caused by the generation of a dominant negative gene product from the mutant ATM allele, because humans heterozygous for different mutations of the ATM gene, including a deletion of the whole ATM locus or missense mutations in the kinase domain, share similar intermediate cellular defects (Lehmann 1982; Shiloh et al. 1985). Heterozygous humans have a somewhat increased cancer rate but none of the other symptoms of AT (Swift et al. 1987, 1991). The defects in radiation response of the heterozygous cells suggest that the increased cancer risk could be attributable to the incomplete cell-cycle arrest and a decreased apoptotic response following DNA damage. The lack of changed cell-cycle parameters in $ATM^{+/-}$ cells suggests that normal cell growth may be less sensitive to the level of ATM than the checkpoint functions and the multiorgan defects such as growth retardation, premature aging, and thymus degeneration in AT patients (Lehman et al. 1982) could be more a consequence of the cell growth defect in $ATM^{-/-}$ cells than the lack of radiation response. The cancer risk in AT heterozygotes, however, could be a direct reflection of the poor radiation response in the heterozygous cells.

ATM regulates the p53 response to ionizing radiation

It has been shown that the cell-cycle arrest in G_1 following DNA damage is mediated by p53 and that DNA damages lead to a rapid and transient increase of p53 protein level (Kastan et al. 1992; Kuerbitz et al. 1992; Lu and Lane 1993). Previous studies to evaluate the p53 response to γ-irradiation in AT cells have yielded conflicting results (Kastan et al. 1992; Lu and Lane 1993). In general agreement with previous reports by Kastan et al. (1992) and Khanna et al. (1993), we found that the p53

response to γ-irradiation in $ATM^{-/-}$ MEFs is substantially defective, indicating that ATM plays a significant role in signaling the p53 response following ionizing irradiation. The delayed kinetics of the p53 response to γ-irradiation we observed in $ATM^{-/-}$ MEFs has also been reported by Lu and Lane (1993) in human AT fibroblasts. However, the greatly reduced p53 response in $ATM^{-/-}$ cells was not observed by Lu and Lane.

γ-irradiation-induced apoptosis of thymocytes is mediated by p53 (Clarke et al. 1993; Lowe et al. 1993). Therefore, the finding that $ATM^{-/-}$ thymocytes, although still sensitive to γ-irradiation, are more resistant to apoptosis induced by γ-irradiation than normal immature thymocytes suggests that the p53 response to DNA damage also may be defective in $ATM^{-/-}$ thymocytes, supporting further the notion that ATM is responsible for signaling the p53 response to DNA-strand-break damage. The resistance of these ATM mutant thymocytes to p53-mediated apoptosis following DNA damage would allow thymocytes harboring damaged DNA to survive and undergo selection for the mutated cells that are neoplastic. This might explain why the predominant tumors found in AT patients are of lymphoid origin (Lehmann 1982). In fact, a greatly increased frequency of thymic lymphomas is now appearing in our $ATM^{-/-}$ mice and these tumors are of $CD4^+CD8^+$ origin (Xu et al., this issue).

Synthesis of p53 protein is regulated negatively by wild-type p53 that binds to the 5′ untranslated region and inhibits the translation of its own mRNA (Mosner et al. 1995). The rapid and transient up-regulation of p53 following DNA damage is mediated through a post-transcriptional mechanism perhaps involving protein stabilization (Kastan et al. 1992; Mosner et al. 1995). In this context, ATM may function by sensing DNA damage and signaling events like relief of the translational inhibition or stabilization of p53. In addition, ATM may carry out its function by directly phosphorylating p53, as suggested by the observation that DNA-PK, a relative of ATM, can phosphorylate p53 in vitro (Hartley et al. 1995).

After this paper was submitted, Barlow et al. (1996) published their description of independently generated ATM mutant mice. Fibroblasts derived from their ATM mutant mice are also defective in both cell-cycle checkpoint control following γ-irradiation and cellular proliferation.

Materials and methods

Cloning of the human ATM cDNA fragment by PCR

A 516-bp cDNA fragment encoding the conserved kinase sequence was amplified from a human B cell cDNA library (gift from S. Elledge, Baylor College of Medicine, Houston, TX) by PCR using primers specific for the human ATM gene (Hunter 1995; Savitsky et al. 1995). The PCR reaction was done in a final volume of 100 μl containing 2 μg of cDNA, 150 ng of each primer, 1× PCR buffer (Boehringer Mannheim), 0.2 mM dNTP, and 5 units of Taq polymerase (Boehringer Mannheim). PCR was run for 35 cycles, each consisting of 1 min at 94°C, 1.5 min

at 62°C and 1 min at 72°C. The final reaction step was followed with an extension at 72°C for 10 min. The PCR product was cloned into the *Bam*HI site of pBluescript SK and verified by DNA sequencing. The sequences of the primers used to amplify the *ATM* cDNA fragment were as follows: 5′-TGCTCATAAA-GGATCCAGGCCAAATGATTT-3′; 5′-AAGAGTGGATCCT-ATAGAACCTCTACAATG-3′.

Targeting construct to disrupt the ATM *gene in ES cells*

The cloned *ATM* cDNA fragment was used as a probe to isolate several murine *ATM* genomic fragments from a mouse 129 genomic library (Strategene) as described previously (Xu et al. 1996b). The exon–intron structure was characterized by restriction mapping, Southern blotting analysis, and DNA sequencing. The mouse protein sequence encoded by the two exons in the genomic fragment is essentially identical to corresponding human protein sequence (Fig. 1A; data not shown). The targeting construct was designed to insert the PGK–neo^r gene into the exon encoding the kinase-conserved sequence and simultaneously to delete the adjacent exon (Fig. 1A,B). The targeting construct was generated by inserting a 1.2-kb *Sal*I–*Sty*I *ATM* genomic fragment into the *Xba*I site 5′ of the PGK-neo^r gene and a 8.5-kb *Xho*I *ATM* genomic fragment into the *Xho*I site 3′ of the PGK-neo^r gene. A 12-kb *Sal*I–*Afl*II DNA fragment was excised out of the targeting construct plasmid and electroporated into J1 ES cells (Fig. 1A,B).

Generation of ATM$^{+/-}$ and ATM$^{-/-}$ ES cells and germ-line transmitting chimeric mice

J1 ES cells were cultured, electroporated, and selected with G418 (300 μg/ml) as described (Li et al. 1992). Homologous recombination events were screened by Southern blotting analysis with *Bam*HI digestion and hybridization to the 1.6-kb probe A, and subsequently confirmed with *Bam*HI digestion and hybridization to the 1.2-kb probe B (Fig. 1A). To generate the *ATM*$^{-/-}$ ES cells, *ATM*$^{+/-}$ ES cells were cultured under increasing concentrations of G418 as described previously (Mortensen et al. 1992; Xu et al. 1996b). Seven *ATM*$^{+/-}$ ES cell-lines were microinjected into C57BL/6 blastocysts that were implanted subsequently into the uteri of Balb/c foster mothers. Male chimeric mice generated from 6 *ATM*$^{+/-}$ ES clones transmitted the *ATM* mutation into germ-line. The presence of the *ATM* mutant allele in the F1 animals was confirmed by Southern blotting. *ATM*$^{+/-}$ F1 animals were bred together to generate *ATM*$^{-/-}$ mice.

Generation and culture of primary MEFs

Primary MEFs were derived from day 14 *ATM*$^{+/+}$, *ATM*$^{+/-}$, and *ATM*$^{-/-}$ embryos as described (Robertson 1987). Genotypes of each MEF culture was verified by Southern blotting. Cells were cultured in Dulbecco's modified Eagle's medium (DMEM) supplemented with 10% fetal calf serum, 5 mM glutamine, 50 μM β-mecaptoethanol, penicillin, and streptomycin at 37°C with 5% CO$_2$.

Analysis of the ATM *mRNA expression with RT–PCR*

Total RNA was isolated from *ATM*$^{+/+}$, *ATM*$^{+/-}$, and *ATM*$^{-/-}$ MEFs using TRI REAGENT following the manufacturer's instruction (Molecular Research Center, Inc.). RT–PCR was carried out as described (Beg et al. 1995). Briefly, 3 μg of total RNA was reverse-transcribed into cDNA and 1 μl of the synthesized cDNA was used in the PCR reaction using three

sets of primers: primers 1 and 2, primers 3 and 4, or primers specific for β-actin. The PCR reaction was done in a final volume of 50 μl containing 150 ng of each primer, 1× PCR buffer, 0.2 mM dNTP, and 2 units of *Taq* polymerase. The PCR reaction went for 30 cycles, each consisting of 1 min at 94°C, 1.5 min at 60°C, and 1.5 min at 72°C. The final reaction step was followed by an extension at 72°C for 10 min. Half of the reaction was analyzed on a 1.2% agarose gel. The sequences of the primers used were as follows: primer 1: 5′-GCTCGTTTATCAAGATA-TTCTGT-3′; primer 2: 5′-AAGTCTTTTGAAGAGAAATAT-GA-3′; primer 3: 5′-AAGAGTGGATCCTATAGAACCTCTA-CAATG-3′; primer 4: 5′-TGCTCATAAAGGATCCAGGCCA-AATGATTT-3′. Sequences for β-actin primers have been described previously (Beg et al. 1995).

Clonogenic survival assay for γ-irradiation

ATM$^{+/+}$, *ATM*$^{+/-}$, and *ATM*$^{-/-}$ ES cells were plated on the MEF feeder layer in a series of six-well plates at a density of 1 × 10^3/well. Twenty hours after plating, ES cells were exposed to graded doses of γ-irradiation with a ^{137}Cs source at a rate of 0.86 Gy/min (1 Gy = 100 rads). The irradiated ES cells were maintained by changing their medium once every 2 days. The surviving ES colonies in each well were counted after 7–8 days of culture.

Irradiation treatment of MEFs and cell-cycle analysis

Asynchronous MEFs were plated at a density of 0.5 × 10^5 to 0.8×10^5 cells per 10-cm plate and irradiated within 24 hr after plating. Fourteen hours after irradiation, cells were pulsed with 10 μM BrdU for 4 hr, harvested, and fixed in 70% ethanol. For γ-irradiation, MEFs were irradiated in the culture medium with a ^{60}Co source at a rate of 4.3 Gy/min. For UV irradiation, culture medium and plate cover were removed before MEFs were irradiated with a UV Stratelinker (Strategene).

For the cell-cycle analysis, DNA synthesis and DNA content were analyzed using flow cytometry as described (Kastan et al. 1992). Briefly, BrdU-labeled cells fixed in 70% ethanol were treated with 1 N HCl containing 0.7% Triton X-100 for 10 min on ice. Subsequently, cells were resuspended in 30 mM HCl, heated at 100°C for 10 min, and transferred back on ice immediately. Cells were incubated with fluorescein isothiocyanate-conjugated anti-BrdU antibodies (Southern Biotech., Inc.), followed by staining with propidium iodide (250 μg/ml) containing RNase (10 μg/ml) overnight. The stained cells were analyzed with a FACscan (Becton-Dickinson) using a CellQuest program as described (Brugarolas et al. 1995).

Protein analysis and antibodies

Immunoblot assays were performed as described (Kastan et al. 1992). Protein extract from 5×10^5 cells was loaded into each lane, separated by 12% SDS–PAGE and transferred to nitrocellulose. After transfer, the membrane was reversibly stained with Ponceau Red to verify the equivalent amount of protein in each lane. The filter was probed with either a monoclonal anti-p53 antibody (P240) or polyclonal anti-p21 antibody obtained from Santa Cruz Biochemicals. The filter was subsequently incubated with horseradish peroxidase-conjugated secondary antibody and developed with enhanced chemiluminescence (ECL) (Amersham).

Radiation-induced thymocyte apoptosis in vivo

Irradiation treatment of animals and analysis of thymocytes were performed as described (Lowe et al. 1993). Briefly, thymo-

cytes were recovered from mice of all genotypes 48 hr after exposure to γ-irradiation (5 Gy) and stained with PE-conjugated anti-CD4 antibody and FITC-conjugated anti-CD8 antibody (both from Pharmingen). As controls, thymocytes from mice without any treatment were also analyzed. Stained cells were analyzed with a FACscan (Becton-Dickinson) using a CellQuest program.

Proliferation assay and analysis of G_1/S transition during the cell-cycle progression

Cell proliferation and saturation density assays were performed essentially as described (Deng et al. 1995), except that three plates were counted at each time point. To synchronize cells at G_0, 70–80% confluent asynchronous culture was washed with PBS and then placed in DMEM containing 0.1% FBS for 96 hr. Cells were harvested and released into DMEM containing 10% FBS and 10 μM BrdU for 24 or 72 hr and harvested. Cells in the S phase were analyzed with flow cytometry as described above.

Acknowledgments

References

Barlow, C., S. Hirotsune, R. Paylor, M. Liyanage, M. Eckhaus, F. Collins, Y. Shiloh, J.N. Crawley, T. Ried, D. Tagle, and A. Wynshaw-Boris. 1996. Atm-deficient mice, a paradigm of ataxia-telangiectasia. *Cell* **86:** 159–171.

Beg, A.A., W.C. Sha, R.T. Bronson, S. Ghosh, and D. Baltimore. 1995. Embryonic lethality and liver degeneration in mice lacking the RelA component of NF-kappa β. *Nature* **376:** 167–170.

Blunt, T., N.J. Finnie, G.E. Taccioli, G.C. Smith, J. Demengeot, T.M. Gottlieb, R. Mizuta, A.J. Varghese, F.W. Alt, P.A. Jeggo, and S.P. Jackson. 1995. Defective DNA-dependent protein kinase activity is linked to V(D)J recombination and DNA repair defects associated with the murine scid mutation. *Cell* **80:** 813–823.

Brown, E.J., P.A. Beal, C.T. Keith, J. Chen, T.B. Shin, and S.L. Schreiber. 1995. Control of p70 s6 kinase by kinase activity of FRAP *in vivo. Nature* **377:** 441–446.

Brugarolas, J., C. Chandrasekaran, J.I. Gordon, D. Beach, T. Jacks, and G.J. Hannon. 1995. Radiation-induced cell cycle arrest compromised by p21 deficiency. *Nature* **377:** 552–557.

Canman, C.E., A.C. Wolff, C.Y. Chen, A.J. Fornace, Jr., and M.B. Kastan. 1994. The p53-dependent G1 cell cycle checkpoint pathways and ataxia-telangiectasia. *Cancer Res.* **54:** 5054–5058.

Carpenter, C.L., K.R. Auger, B.C. Duckworth, W.M. Hou, B. Schaffhausen, and L.C. Cantley. 1993. A tightly associated

serine/threonine kinase regulates phosphoinositide 3-kinase activity. *Mol. Cell. Biol.* **13:** 1657–1665.

Clarke, A.R., C.A. Purdie, D.J. Harrison, R.G. Morris, C.C. Bird, M.L. Hooper, and A.H. Wylie. 1993. Thymocyte apoptosis induced by p53-dependent and independent pathways. *Nature* **362:** 849–852.

Deng, C., P. Zhang, J.W. Harper, S.J. Elledge, and P. Leder. 1995. Mice lacking p21CIP1/WAF1 undergo normal development, but are defective in G1 checkpoint control. *Cell* **82:** 675–684.

Dhand, R., I. Hiles, G. Panayotou, S. Roche, M.J. Fry, I. Gout, N.F. Totty, O. Truong, P. Vicendo, K. Yonezawa, M. Kasuga, S.A. Courtneidge, and M.D. Waterfield. 1994. PI 3-kinase is a dual specificity enzyme: Autoregulation by an intrinsic protein-serine kinase activity. *EMBO J.* **13:** 522–533.

El-Deiry, W.S., T. Tokino, V.E. Velculescu, D.B. Levy, R. Parsons, J.M. Trent, D. Lin, W.E. Mercer, K.W. Kinzler, and B. Vogelstein. 1993. WAF1, a potential mediator of p53 tumor suppression. *Cell* **75:** 817–825.

Greenwell, P.W., S.L. Kronmal, S.E. Porter, J. Gassenhuber, B. Obermaier, and T.D. Petes. 1995. TEL1, a gene involved in controlling telomere length in S. cerevisiae, is homologous to the human ataxia telangiectasia gene. *Cell* **82:** 823–829.

Halevy, O., B.G. Novitch, D.B. Spicer, S.X. Skapek, J. Rhee, G.J. Hannon, D. Beach, and A.B. Lassar. 1995. Correlation of terminal cell cycle arrest of skeletal muscle with induction of p21 by MyoD. *Science* **267:** 1018–1021.

Hari, K.L., A. Santerre, J.J. Sekelsky, K.S. McKim, J.B. Boyd, and R.S. Hawley. 1995. The mei-41 gene of D. melanogaster is a structural and functional homolog of the human ataxia telangiectasia gene. *Cell* **82:** 815–821.

Hartley, K.O., D. Gell, G.C. Smith, H. Zhang, N. Divecha, M.A. Connelly, A. Admon, S.P. Lees-Miller, C.W. Anderson, and S.P. Jackson. 1995. DNA-dependent protein kinase catalytic subunit: A relative of phosphatidylinositol 3-kinase and the ataxia telangiectasia gene product. *Cell* **82:** 849–856.

Hunter, T. 1995. When is a lipid kinase not a lipid kinase? When it is a protein kinase. *Cell* **83:** 1–4.

Kastan, M.B., O. Onyekwere, D. Sidransky, B. Vogelstein, and R.W. Craig. 1991. Participation of p53 protein in the cellular response to DNA damage. *Cancer Res.* **51:** 6304–6311.

Kastan, M.B., Q. Zhan, W.S. El-Deiry, F. Carrier, T. Jacks, W.V. Walsh, B.S. Plunkett, B. Vogelstein, and A.J. Fornace, Jr. 1992. A mammalian cell cycle checkpoint pathway utilizing p53 and GADD45 is defective in ataxia-telangiectasia. *Cell* **71:** 587–597.

Khanna, K.K. and M.F. Lavin. 1993. Ionizing radiation and UV induction of p53 protein by different pathways in ataxiatelangiectasia cells. *Oncogene* **8:** 3307–3312.

Kuerbitz, S.J., B.S. Plunkett, W.V. Walsh, and M.B. Kastan. 1992. Wild-type p53 is a cell cycle checkpoint determinant following irradiation. *Proc. Natl. Acad. Sci.* **89:** 7491–7495.

Lehmann, A.R. 1982. Ataxia-Telangiectasia: A cellular and molecular link between cancer, neuropathology and immune deficiency (ed. B.A. Bridges and D.G. Harnden), pp. 83–102. Wiley, Chichester, UK.

Li, E., T.H. Bestor, and R. Jaenisch. 1992. Targeted mutation of the DNA methyltransferase gene results in embryonic lethality. *Cell* **69:** 915–926.

Lowe, S.W., E.M. Schmitt, S.W. Smith, B.A. Osborne, and T. Jacks. 1993. p53 is required for radiation-induced apoptosis in mouse thymocytes. *Nature* **362:** 847–849.

Lu, X. and D.P. Lane. 1993. Differential induction of transcriptionally active p53 following UV or ionizing radiation: Defects in chromosome instability syndromes? *Cell* **75:** 765–778.

Macleod, K.F., N. Sherry, G. Hannon, D. Beach, T. Tokino, K. Kinzler, B. Vogelstein, and T. Jacks. 1995. p53-dependent and independent expression of p21 during cell growth, differentiation, and DNA damage. *Genes & Dev.* **9:** 935–944.

Meyn, M.S. 1995. Ataxia-Telangiectasia and cellular responses to DNA-damage. *Cancer Res.* **55:** 5991–6001.

Morrow, D.M., D.A. Tagle, Y. Shiloh, F.S. Collins, and P. Hieter. 1995. TEL1, an S. cerevisiae homolog of the human gene mutated in ataxia telangiectasia, is functionally related to the yeast checkpoint gene MEC1. *Cell* **82:** 831–840.

Mortensen, R.M., D.A. Conner, S. Chao, A.A. Geisterfer-Lowrance, and J. G. Seidman. 1992. Production of homozygous mutant ES cells with a single targeting construct. *Mol. Cell. Biol.* **12:** 2391–2395.

Mosner, J., T. Mummenbrauer, C. Bauer, G. Sczakiel, F. Grosse, and W. Deppert. 1995. Negative feedback regulation of wild-type p53 biosynthesis. *EMBO J.* **14:** 4442–4449.

Nakanishi, M., G.R. Adami, R.S. Robertorye, A. Noda, S.F. Venable, D. Dimitrov, O.M. Pereira-Smith, and J.R. Smith. 1995. Exit from G_0 and entry into the cell cycle of cells expressing p21^{Sdi1} antisense RNA. *Proc. Natl. Acad. Sci.* **92:** 4352–4356.

Parker, S.B., G. Eichele, P. Zhang, A. Rawls, A.T. Sands, A. Bradley, E.N. Olson, J.W. Harper, and S.J. Elledge. 1995. p53-independent expression of p21^{Cip1} in muscle and other terminally differentiating cells. *Science* **267:** 1024–1027.

Paulovich, A.G. and L.H. Hartwell. 1995. A checkpoint regulates the rate of progression through S phase in S. cerevisiae in response to DNA damage. *Cell* **82:** 841–847.

Robertson, E.J. 1987. Embryo-derived stem cell lines. In *Teratocarcinomas and embryonic stem cells: A practical approach* (ed. E.J. Robertson), pp. 71–112. IRL Press, Oxford, UK.

Savitsky, K., A. Bar-Shira, S. Gilad, G. Rotman, Y. Ziv, L. Vanagaite, D.A. Tagle, S. Smith, T. Uziel, S. Sfez, M. Ashkenazi, L. Pecker, M. Frydman, R. Harnik, R.P. Sankhavaram, A. Simmons, G.A. Clines, A. Sartiel, R.A. Gatti, L. Chessa, O. Sanal, M.F. Lavin, N.G.J. Jaspers, M.R. Taylor, C.F. Arlett, T. Miki, S.M. Weissman, M. Lovett, F. Collins, and Y. Shiloh. 1995. A single ataxia telangiectasia gene with a product similar to PI-3 kinase. *Science* **268:** 1749–1753.

Shiloh, Y., E. Tabor, and Y. Becker. 1985. *In vitro* phenotype of ataxia-telangiectasia (AT) fibroblast strains: Clues to the nature of the "AT DNA lesion" and the molecular defect in AT. *Kroc Found. Ser.* **19:** 111–121.

Smith, C.A., G.T. Williams, R. Kingston, E.J. Jenkinson, and J.J. Owen. 1989. Antibodies to CD3/T-cell receptor complex induce death by apoptosis in immature T cells in thymic cultures. *Nature* **337:** 181–184.

Swift, M., P.J. Reitnauer, D. Morrell, and C.L. Chase. 1987. Breast and other cancers in families with ataxia-telangiectasia. *N. Engl. J. Med.* **316:** 1289–1294.

Swift, M., D. Morrell, R.B. Massey, and C.L. Chase. 1991. Incidence of cancer in 161 families affected by ataxia-telangiectasia. *N. Engl. J. Med.* **325:** 1831–1836.

Thacker, J. 1994. Cellular radiosensitivity in ataxia-telangiectasia. *Int. J. Radiat. Biol.* **66:** S87–96.

Weinert, T. and D. Lydall. 1993. Cell cycle checkpoints, genetic instability and cancer. *Semin. Cancer Biol.* **4:** 129–140.

Xiong, Y., G.J. Hannon, H. Zhang, D. Casso, R. Kobayashi, and D. Beach. 1993. p21 is a universal inhibitor of cyclin kinases. *Nature* **366:** 701–704.

Xu, Y., T. Ashley, E.E. Brainerd, R.T. Bronson, M.S. Meyn, and D. Baltimore. 1996a. Targeted disruption of ATM leads to growth retardation, chromosomal fragmentation during meiosis, immune defects, and thymic lymphoma. *Genes & Dev.* (this issue).

Xu, Y., L. Davidson, F.W. Alt., and D. Baltimore. 1996b. Deletion of the Igκ light chain intronic enhancer/matrix attachment region impairs but does not abolish VκJκ rearrangement. *Immunity* **4:** 377–385.

Zakian, V.A. 1995. *ATM*-related genes: What do they tell us about functions of the human gene? *Cell* **82:** 685–687.

References	This article cites 41 articles, 11 of which can be accessed free at: **http://genesdev.cshlp.org/content/10/19/2401.full.html#ref-list-1**
License	
Email Alerting Service	Receive free email alerts when new articles cite this article - sign up in the box at the top right corner of the article or **click here.**